The simulation results are seen to be in good agreement with measured values.

The fundamental gain of the FET falls with frequency at 6 dB per octave, and therefore a similar fall in frequency doubler conversion gain (the ratio of second harmonic output power to fundamental input power) of the FET is expected. However, parasitics and transit time effects may increase the rate of fall off. Thus the maximum value of doubler conversion gain is expected to become negative above the frequency at which the device fundamental gain falls below about 6 dB. These predictions are confirmed by Fig. 2, which shows the computed variation in fundamental and doubler conversion gain with frequency and drive level, for the FET modeled earlier.

III. Dual-Gate FET Doubler

The dual-gate FET can be modeled as two single-gate FET's in series; a grounded-source device associated with gate 1, which is adjacent to the source, and a grounded-gate device associated with gate 2, which is adjacent to the drain. However, the behavior of this structure as a doubler is more readily discerned by treating the FET as a three-terminal device, with the second gate appropriately terminated. The $I_d - V_{ds}$ characteristics of this device are similar in form to those of the single-gate FET but with the second gate bias determining the maximum saturated current. A suitable load line construction then provides a guide to the doubler behavior.

The two major sources of nonlinearity in the single-gate FET, the I_d clipping and the $V_{gs} - I_d$ transfer nonlinearity, may be accounted for in the dual-gate device on this basis. Using similar arguments to the single-gate FET, the dual-gate doubler conversion gain is about 6 to 8 dB below the corresponding input frequency fundamental gain when gate 1 is biased close to saturation and/or forward conduction, or to pinchoff, and about 12 dB lower than the fundamental gain when biased midway between pinchoff and forward conduction. As in the single-gate FET, the input gate junction is inefficient as a varactor harmonic generator, and the output slope conductance nonlinearity also does not generate significant second harmonic power. Thus the mechanisms determining the performance of the dual-gate FET doubler are similar to those for the single-gate doubler.

However, since the dual-gate FET has a small signal gain which is typically 6 dB higher than that for a comparable single-gate device, the dual-gate FET doubler conversion gain is increased by a corresponding amount. This increased gain can be seen in Fig. 3, which shows large signal simulation results for a dual-gate FET, comprising two of the single-gate devices modeled previously connected in series. The series connection of FET's gives a lower power handling capability for the dual-gate device than for the single-gate FET with equal V_{ds}. Consequently, fundamental and doubler conversion gains peak at lower values of input power. As predicted, the maximum value of dual-gate doubler conversion gain is about 6 dB less than the fundamental gain, the difference decreasing at higher input powers, with the onset of saturation. Such behavior is also shown by the single-gate device (see Fig. 2). Comparison with Fig. 2 shows that the maximum values of doubler conversion gain are 6 to 8 dB higher than those for the single-gate FET, in agreement with earlier predictions. The fundamental and doubler conversion gains fall by about 9 dB as the input frequency is increased from 4 to 8 GHz. Experimental results of Chen *et al.* [2] show similar trends to those of Fig. 3.

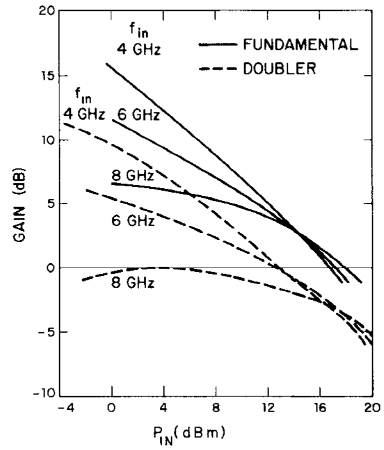

Fig. 3. Computed variation in fundamental and doubler conversion gain with frequency and drive level for dual-gate FET $V_{ds} = 5$ V, $V_{g1s} = -1.5$ V, $V_{g2s} = 2$ V.

Conclusions

The paper has shown that the observed performance characteristics of single-and dual-gate FET frequency doublers are adequately described on the basis of simple analytical considerations. The apparent superior performance of the dual-gate FET doubler is found to be largely a result of the higher intrinsic device gain rather than of any increased nonlinearity.

References

[1] M. S. Gupta, R. W. Laton, and T. T. Lee, "Frequency multiplication with high power microwave field-effect transistors," in *IEEE MTT-S Int. Microwave Symp. Digest*, pp. 498–500, 1979.

[2] P. T. Chen, C. T. Li, and P. H. Wang, "Performance of a dual-gate GaAs MESFET as a frequency multiplier at *Ku*-band," *IEEE Trans. Microwave Theory Tech*, vol. MTT-27, pp. 411–415, May 1979.

[3] R. Stancliff, "Balanced dual-gate GaAs FET frequency doublers," in *IEEE MTT-S Int Microwave Symp. Digest*, pp. 143–145, 1981.

[4] P. Penfield and R. P. Rafuse, *Varactor Applications* Cambridge, MA: M.I.T. Press, 1962.

[5] A. Gopinath, A. J. Seeds, J. B. Rankin, and R. W. Sudbury, "Performance of MESFET frequency multipliers," in *Proc. Eighth Biennial Cornell Electrical Engineering Conf*, 1981.

Quasi-Static Characteristics of Coplanar Waveguide on a Sapphire Substrate with Its Optical Axis Inclined

TOSHIHIDE KITAZAWA AND YOSHIO HAYASHI

***Abstract*— A variational expression is presented for the line capacitance of a coplanar waveguide on a single-crystal sapphire substrate with a tilted optical axis. Numerical results are obtained by means of the Ritz procedure.**

Manuscript received November 24, 1981; revised January 4, 1982.
The authors are with the Department of Electronic Engineering, Kitami Institute of Technology, Kitami (090), Japan

0018-9480/82/0600-0920$00.75 ©1982 IEEE

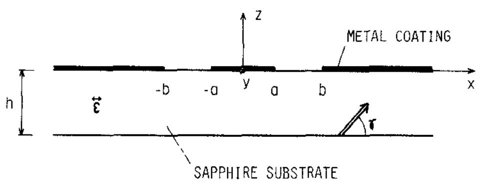

Fig. 1. Coplanar waveguide (CPW).

The transmission lines on an anisotropic substrate have been studied for use in MIC [1], [2]. Recently, coupled slots on a single-crystal sapphire substrate cut with its planar surface perpendicular to the optical axis have been investigated and the variational expression of the line capacitance has been derived for the odd mode of the coupled slots, that is, the coplanar waveguide (CPW) [3]. In this short paper, we extend this approach to obtain a variational expression of the line capacitance of the CPW on an anisotropic sapphire substrate when its optical axis lies in the transverse plane but is not coincident with one of the coordinate axes (Fig. 1). The permittivity tensor of this anisotropic substrate is given by the following dyadic:

$$\overleftrightarrow{\varepsilon}=\varepsilon_0\begin{bmatrix}\varepsilon_{xx} & 0 & \varepsilon_{xz}\\ 0 & \varepsilon_{yy} & 0\\ \varepsilon_{xz} & 0 & \varepsilon_{zz}\end{bmatrix} \tag{1}$$

where

$$\varepsilon_{xx}=\varepsilon_{\parallel}\cos^2\gamma+\varepsilon_{\perp}\sin^2\gamma$$
$$\varepsilon_{yy}=\varepsilon_{\perp}$$
$$\varepsilon_{zz}=\varepsilon_{\parallel}\sin^2\gamma+\varepsilon_{\perp}\cos^2\gamma$$
$$\varepsilon_{xz}=(\varepsilon_{\parallel}-\varepsilon_{\perp})\sin\gamma\cos\gamma$$
$$\varepsilon_{\parallel}=11.6,\qquad \varepsilon_{\perp}=9.4$$

where γ is the angle of the optical axis from the x axis.

Under a quasi-static approximation, we extend the method used in [3], and obtain a stationary expression of the line capacitance per unit length of the CPW on this anisotropic substrate

$$C=\frac{\int_a^b\int_a^b\int_0^\infty e_x(x)G(\alpha;x|x')e_x(x')\,d\alpha\,dx'\,dx}{\left\{\int_a^b e_x(x)\,dx\right\}^2} \tag{2}$$

$$G(\alpha;x|x')=\frac{4\varepsilon_0}{\pi}\left\{1+\frac{1+\varepsilon_e\tanh(Kh\alpha)}{1+\frac{1}{\varepsilon_e}\tanh(Kh\alpha)}\right\}\frac{1}{\alpha}\sin\alpha x\sin\alpha x'$$

$$K=\sqrt{\frac{\varepsilon_{xx}}{\varepsilon_{zz}}-\left(\frac{\varepsilon_{xz}}{\varepsilon_{zz}}\right)^2}=\frac{\sqrt{\varepsilon_{\perp}/\varepsilon_{\parallel}}}{1+\left(\frac{\varepsilon_{\perp}}{\varepsilon_{\parallel}}-1\right)\cos^2\gamma}$$

$$\varepsilon_e=\sqrt{\varepsilon_{xx}\varepsilon_{zz}-\varepsilon_{xz}^2}=\sqrt{\varepsilon_{\parallel}\varepsilon_{\perp}}$$

where $e_x(x)$ is the unknown field distribution at the slot surface $z=0$. Equation (2) provides the upper bound on the line capacitance. Equation (2) shows that the line capacitance of the CPW on this anisotropic substrate is identical with that of the CPW on the equivalent isotropic substrate with effective height $K\cdot h$ and relative permittivity ε_e.

Numerical results are obtained by applying the Ritz procedure to the variational expression (2). In this procedure, we express the unknown slot field $e_x(x)$ as

$$e_x(x)=f_0(x)+\sum_{k=1}^{N}A_kf_k(x) \tag{3}$$

$$f_k(x)=\frac{T_k\left\{\frac{2(x-S)}{W}\right\}}{\sqrt{1-\left\{\frac{2(x-S)}{W}\right\}^2}},\qquad W=b-a,\quad S=(a+b)/2$$

where $T_k(y)$ are Chebyshev's polynomials of the first kind and A_k are variational parameters. The basis functions $f_k(x)$ in the above expansion satisfy the appropriate edge conditions.

Table I shows the numerical results of the normalized line capacitance $(\pi/4\varepsilon_0)C$ of the CPW for different values of N in (3). The analytical solution can be obtained only for the structure without substrate ($\varepsilon_{\parallel}=\varepsilon_{\perp}=1$), and for such a case the values obtained by conformal mapping are presented.

Fig. 2 shows the effective dielectric constant ε_{eff} and the characteristic impedance Z_0 of the CPW on a sapphire substrate cut with its surface at γ (degrees) to the optical axis.

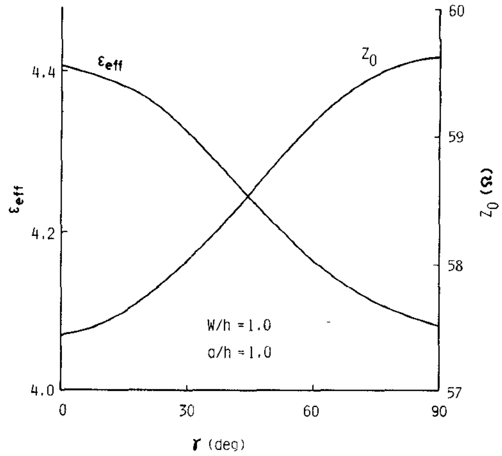

Fig. 2. Effective dielectric constant ε_{eff} and characteristic impedance Z_0 versus γ.

TABLE I
LINE CAPACITANCE OF CPW $(\pi/4\varepsilon_0)C$

a/b \ N	0	1	2	Conformal mapping
0.2	1.7273	1.6547	1.6529	1.6529
0.4	2.2093	2.1840	2.1838	2.1838
0.6	2.7646	2.7566	2.7566	2.7566
0.8	3.5820	3.5804	3.5804	3.5804

$\varepsilon_{\parallel}=\varepsilon_{\perp}=1.0$, $h=0$

a/b \ N	0	1	2	3
0.2	8.4761	8.3046	8.3009	8.3005
0.5	10.4229	10.4160	10.4150	10.4150

$\varepsilon_{\parallel}=11.6$, $\varepsilon_{\perp}=9.4$, $\gamma=\pi/4$
$W/h=1$, $W=b-a$

In conclusion, a variational expression is presented for the line capacitance of the CPW on a single-crystal sapphire substrate with its optical axis inclined. Numerical results by the Ritz procedure are also presented.

References

[1] N. G. Alexopoulos and C M Krowne, "Characteristics of single and coupled microstrips on anisotropic substrates," *IEEE Trans. Microwave Theory Tech.*, vol. MTT-26, pp. 387–393, June 1978.

[2] M. Kobayashi and R. Terakado, "New view on an anisotropic medium and its application to transformation from anisotropic to isotropic problems," *IEEE Trans. Microwave Theory Tech.*, vol. MTT-27, pp. 769–775, Sept. 1979.

[3] T Kitazawa and Y Hayashi, "Coupled slots on an anisotropic sapphire substrate," *IEEE Trans Microwave Theory Tech.*, vol. MTT-29, pp. 1035–1040, Oct. 1981

Nonreciprocal Propagation Characteristics of YIG Thin Film

TETSUYA MIZUMOTO, STUDENT MEMBER, IEEE, AND YOSHIYUKI NAITO, SENIOR MEMBER, IEEE

Abstract —**The characteristics of an optical nonreciprocal phase shifter, with which optical circulators can be constructed, are investigated. We have measured the nonreciprocal phase shift of an appropriately magnetized yttrium iron garnet (YIG) thin film and thus confirmed experimentally that an AIR/YIG/GGG structure can function as an optical nonreciprocal phase shifter.**

I. Introduction

Nonreciprocal devices, such as isolators and circulators, are necessary in optical communication systems in order to avoid self-oscillation due to reflections in the laser amplifier. At present, we can get optical isolators of practically good performance only in a bulk form. However, they are not realized in a thin-film waveguide form which is compatible with integrated optical circuits in the future systems. Several workers have investigated thin-film optical isolators using unidirectional TE–TM mode conversion in magnetooptic materials [1]–[4], but their results are considerably unsatisfactory. The difficulties arise from the following reasons. 1) It is necessary to use anisotropic materials, such as $LiNbO_3$ or $LiIO_3$, in a proper way. But, these materials cannot be grown on magnetic materials because of their lattice mismatch. Besides, the gap between the anisotropic material and the thin film is a critical factor and it is almost impossible to get a uniform optical contact over a long distance. 2) It is required to control the thickness of thin films very accurately. Typically, the accuracy of 0.1 percent to 1.0 percent of the optical wavelength is required. These two requirements are necessary to make the TE and TM modes phase match, which is inevitable if unidirectional TE–TM mode conversion in a magnetooptic material is used.

By the way, a different type of the optical circulator, which makes use of nonreciprocal phase shift in magnetooptic materials for TM modes, has been proposed [5]. The advantages of this structure are: 1) no need of phase matching, therefore no need of anisotropic materials and higher tolerances of the film thickness; and 2) ease of excitation of eigenmodes as they are pure TM modes.

We observed that the TM_0 mode suffers a nonreciprocal phase shift in a properly magnetized YIG thin film. In Section II, we treat theoretically the optical nonreciprocal phase shifter, which is the important part of the optical circulator. Next we also show the results of measurement of nonreciprocal phase shift in Section III.

II. Optical Nonreciprocal Phase Shifter (ONPS)

The schematic diagram of the optical circulator using ONPS is shown in Fig. 1. This circuit functions as follows. A wave entering waveguide 1 from the left is split into two waves of equal amplitudes by means of the 3-dB coupler I. The two waves then propagate in the two waveguides, one of which is ONPS, and are again combined by means of the 3-dB coupler II. With proper selection of parameters we can design this structure in such a way that behind the second 3-dB coupler all the energy is guided in only one waveguide (e.g., in waveguide 4). If ONPS is designed in such a manner that forward and reverse traveling waves have phase shifts different by π, then for the reverse traveling wave from waveguide 4 all the energy will be coupled into waveguide 2, not into waveguide 1. Similarly, a wave entering waveguide 2 from the left comes out in waveguide 3, and the reverse traveling wave from waveguide 3 goes to waveguide 1.

ONPS consists of an asymmetric three-layer waveguide structure (Fig. 2). Each medium is assumed to be a lossless magnetooptic material with dielectric tensor

$$\tilde{\epsilon}_i = \epsilon_0 \begin{pmatrix} \epsilon_i & 0 & 0 \\ 0 & \epsilon_i & j\alpha_i \\ 0 & -j\alpha_i & \epsilon_i \end{pmatrix} \qquad (i=1,2,3).$$

It is said that there exists magnetic birefringence in the bulk case of YIG [6]. Here, we neglect it because it is considered relatively small compared to the magnetooptic anisotropy. The dc magnetizing field is applied in the X-axis direction. And the wave propagates in the Z-axis direction. We solve the exact eigenvalue equation for this structure [7] and obtain the characteristic equation for the TM modes

$$\tan(kd) = \frac{\dfrac{k}{\epsilon_2'}\left\{\dfrac{p}{\epsilon_1'} + \dfrac{q}{\epsilon_3'} + \left(\dfrac{\alpha_1}{\epsilon_1\epsilon_1'} - \dfrac{\alpha_3}{\epsilon_3\epsilon_3'}\right)\beta\right\}}{C_0 + C_1\beta + C_2\beta^2} \qquad (1)$$

where

$$C_0 = \left(\frac{k}{\epsilon_2'}\right)^2 - \frac{p}{\epsilon_1'}\frac{q}{\epsilon_3'}$$

$$C_1 = \frac{p}{\epsilon_1'}\left(\frac{\alpha_3}{\epsilon_3\epsilon_3'} - \frac{\alpha_2}{\epsilon_2\epsilon_2'}\right) + \frac{q}{\epsilon_3'}\left(\frac{\alpha_2}{\epsilon_2\epsilon_2'} - \frac{\alpha_1}{\epsilon_1\epsilon_1'}\right)$$

$$C_2 = \left(\frac{\alpha_2}{\epsilon_2\epsilon_2'} - \frac{\alpha_1}{\epsilon_1\epsilon_1'}\right)\left(\frac{\alpha_2}{\epsilon_2\epsilon_2'} - \frac{\alpha_3}{\epsilon_3\epsilon_3'}\right)$$

$$\epsilon_i' = (\epsilon_i^2 - \alpha_i^2)/\epsilon_i$$

$$\beta^2 = \epsilon_1' k_0^2 + p^2 = \epsilon_2' k_0^2 - k^2 = \epsilon_3' k_0^2 + q^2 \qquad (k_0^2 = \omega^2\epsilon_0\mu_0).$$

β represents the propagation constant in the Z-axis direction. Because of nonzero linear terms in β, this equation shows that

Manuscript received September 14, 1981; revised December 30, 1981

The authors are with the Department of Electrical and Electronics Engineering, Tokyo Institute of Technology, Meguro-ku, Tokyo 152, Japan.

0018-9480/82/0600-0922$00.75 ©1982 IEEE